J. Fluid Mech. (1973), *vol.* 57, *part* 3, *pp.* 583–602
Printed in Great Britain

Some aspects of fully developed turbulent flow in non-circular ducts

By S. C. KACKER

Department of Mechanical Engineering, University of Newcastle-upon-Tyne

(Received 31 January 1972 and in revised form 14 July 1972)

An experimental study of fully developed uniform-density turbulent flow in a circular pipe containing one or two rods located off-centre is described. The friction factor in both cases was found to be approximately 5 % higher than the simple pipe friction factor. The shear stress distribution on the rod surface was determined using calibrated boundary-layer fences. The normalized shear stress distributions were independent of Reynolds number in the range $3{\cdot}7 \times 10^4$ to $2{\cdot}15 \times 10^5$. Mean-velocity measurements were obtained to check the validity of the universal law of the wall near the rod surface. Secondary-flow velocities were measured by a hot-wire anemometer and integrated to yield the secondary-flow stream function. Secondary-flow velocities of the order of 1 % of the mean velocity were observed. In the gap between the two pins, however, the secondary-flow velocities were only $\frac{1}{2}$ % of the mean velocity. It is demonstrated that the secondary flow cannot be neglected if a force balance is used to determine the shear stress distribution on the rod surface.

1. Introduction

The coolant channels of several designs of nuclear reactor contain clusters of fuel pins. Knowledge of the flow in such a cluster is still far from adequate. Recent work on square ducts (Hoagland 1960; Brundrett & Baines 1964; Gessner & Jones 1965; Ying 1971) represents an important step towards improving the understanding of the flow in a reactor cluster. This is because the possible importance of secondary flows and their influence on other flow parameters such as the mean velocity, friction factor and Stanton number has been recognized (Skinner, Freeman & Lyall 1969). As yet, no satisfactory analysis exists which would predict the magnitude of secondary flows in a cluster or in simple non-circular ducts such as the square duct, elliptical duct or eccentric annulus; but for the particular case of the square duct, Ying (1971) developed a program which is capable of predicting the secondary flows, provided that the turbulence structure is fed in as an input. There is also disagreement in the literature on the law of the wall for the velocity profile over slender cylinders; obviously, such information is of great importance in predicting the friction factor and heat-transfer coefficients for fuel pins. In view of the lack of successful theoretical models, it remains for experimental investigation to provide the information needed.

In the present study, fully developed turbulent flow in a circular pipe containing one or two rods located off-centre is examined. The main objective was to gain further knowledge concerning the variation of skin friction around the periphery of the pipe and the rods (also referred to as pins in the text), and to test the validity of the law of the wall for the velocity profile near the pin surface. Secondary-flow velocities were experimentally measured using a technique similar to that used by Hoagland (1960). The question of how the presence of one pin influences the flow near the second pin is examined.

Jonsson & Sparrow (1966) presented a comprehensive experimental study of turbulent flow in eccentric annular ducts. Although the present study describes experimental results for only one eccentricity, it has been possible to examine the assumptions made by Jonsson & Sparrow in the calculation of the shear stress variation around the pins; this is of considerable importance as the correct formulation of the law of the wall depends upon the precision of the calculated shear stress.

2. The experimental apparatus

The geometry of the duct under consideration is shown in figure 1. In the single-pin experiment a 1 in. diameter rod was located in a 5·683 in. diameter pipe. The distance s between the centres of the pin and the pipe was 1·113 in., which gave an eccentricity $e = s/(R_p - R_r) = 0{\cdot}475$, where R_p and R_r are radius of curvature of the pipe and rod respectively. In the two-pin experiment, a second rod was located symmetrically opposite the first rod. The total length of the assembly was approximately 308 in., which gave development lengths for the single-pin and two-pin experiments of about 67 and 78 hydraulic diameters respectively. The working fluid was air at atmospheric temperature and pressure.

The layout of the test assembly is shown in figure 2. The test rig is similar to the one used by Lawn & Elliott (1972), who carefully checked the accuracy of the open-orifice flow metering device. For the details of the rig design, the reader should refer to Lawn (1970) and Kacker (1971). In this section only important modifications to the rig will be described.

The last two pipe sections of the rig were designed to enable probes to be traversed in any radial direction. The test section was provided with a traversing port in the centre of the duct through which either a Pitot tube or a hot-wire probe could be introduced. Traverses could be made either using a hand-operated micrometer or an automatic traversing gear (a DISA 52 BO 1 sweep drive unit together with a DISA 55 HO 1 traversing mechanism and a 52 CO 1 stepper motor). A protractor was fitted on the flange of the 18 in. long section. The traversing section could be rotated about its axis and its position could be recorded on the protractor.

To make the traverses normal to the pin, the probe was introduced from the top of the test section. The probe was held in a vernier ring which was clamped onto a support concentric with the pipe. The vernier ring had slots cut in such a way as to allow traversing normal to the pin.

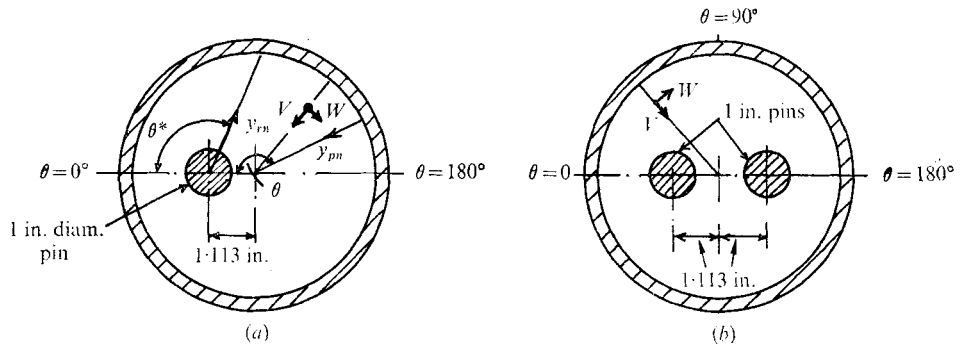

FIGURE 1 Geometry of the ducts. 5·683 in. I.D. pipe (thickness $\frac{9}{32}$ in.). Flow coming out of the plane of the paper. Not to scale. (*a*) One-pin experiment. (*b*) Two-pin experiment.

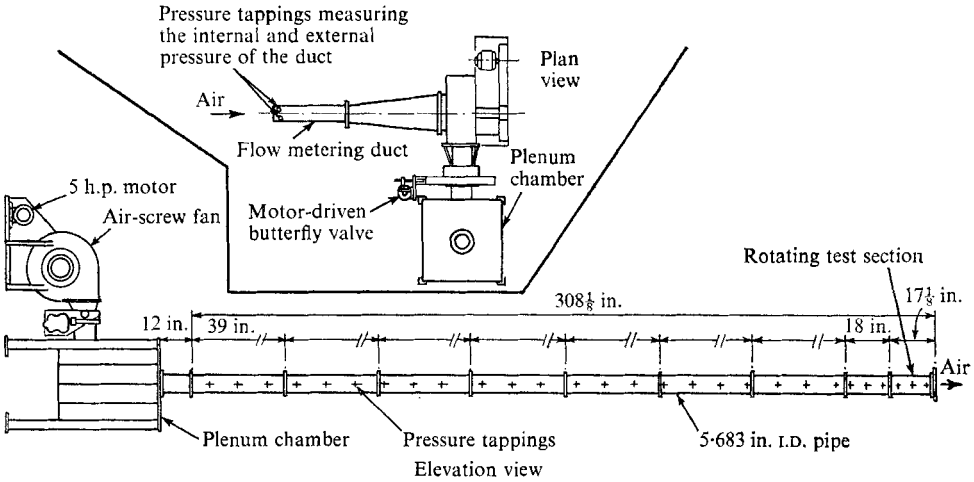

FIGURE 2. Layout of the experiment.

3. Measurement techniques

3.1. *Velocity measurements*

Mean velocities were measured using a double Pitot tube. The distance between the heads, which had outer diameters of $\frac{1}{32}$ in., was approximately 0·275 in. MacMillan's (1956) correction for displacement of the effective centre of the Pitot tube was applied to all the velocity readings. Pressures were recorded by an air flow manometer or pressure transducer (type MDC-Furness Control Ltd).

3.2. *Skin-friction sleeve*

A velocity profile near a plane surface is usually represented by a law of the wall having the following functional form:

$$U^+ = f(y^+), \tag{1}$$

where $U^+ = U/u_\tau$, $y^+ = yu_\tau/\nu$, $u_\tau = (\tau_s/\rho)^{\frac{1}{2}}$, U is the mean velocity parallel to the duct axis, y distance normal to a surface, τ_s the wall shear stress, ρ the fluid

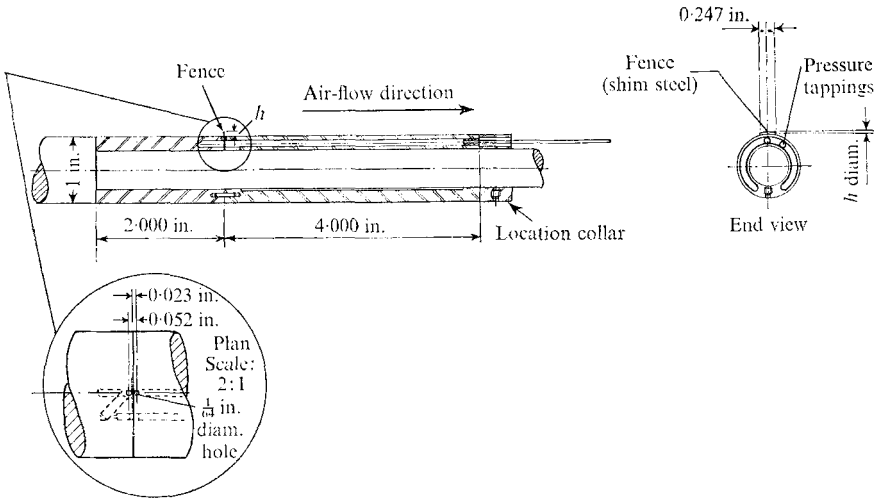

FIGURE 3. Design of the skin-friction sleeve.

Fence code name	$A1$	$A2$	$A3$	$A4$
Dimension, h (in.)	0·0083	0·0026	0·0043	0·0057

density and ν the kinematic viscosity. There is sufficient experimental evidence (Rao 1967; Starr & Sparrow 1967; Lawn & Elliot 1972) to suggest that the law of the wall holds only very near the pin surface, probably because the approximation of constant shear stress is a poor one beyond a certain value of y/R, where R is the radius of curvature of the surface in question (see § 4.3). Consequently, it would be wrong to use any skin-friction measuring device (such as a Preston tube) which depends upon the knowledge of the universal velocity profile. In the present experiments, a boundary-layer fence was used to determine the shear stress. The height of the fence was small enough for it to be sensitive to the velocity profile in the viscous sublayer only. The law of the wall is likely to be more universal in the viscous region than either in the transition region or in the logarithmic region.

The design of the skin-friction sleeve incorporating the fence is shown in figure 3. Four sleeves $A1$, $A2$, $A3$ and $A4$ having fence heights of 0·0083 in., 0·0026 in., 0·0043 in. and 0·0057 in. were constructed. The pressure difference across the fence was carefully measured with a micromanometer (Combustion Instruments Ltd, type 'Combist'). It is estimated that the micromanometer is accurate to within $\pm$ 0·0002 in. of water.

3.3. *Secondary-flow meter*

Previous studies of the flow in square ducts (Hoagland 1960; Brundrett & Baines 1964; Gessner & Jones 1965; Ying 1971) have shown that the secondary velocities are of the order of 1 or 2 % of the mean flow. A hot-wire technique suggested by Hoagland (1960) has been used by these workers and has been found to be sensitive enough for the measurement of small secondary velocities. In the present experiments, a secondary-flow meter designed by Hollingsworth (1967) on the lines suggested by Hoagland (1960) was used. Ying (1971) used the same

secondary-flow meter in a square duct and found that his results were in agreement with those of other workers. A new traversing system was designed for the meter in order to facilitate traversing in the present test section.

Symmetry requires that the secondary-flow velocity W (see figure 1) be zero everywhere on the lines of symmetry $\theta = 0, 180°$, where θ is the azimuthal angle measured at the centre of the pipe. It was found that there was some scatter in the secondary-flow angle γ (defined by equation (6)) at $\theta = 0$ and therefore γ was measured relative to the direction $\theta = 180°$. The sensor of the hot-wire probe (DISA type 55F11) was a 0·118 in. long, 0·0002 in. diameter Pt-plated tungsten wire which was gold-plated at the ends to a thickness of 0·0012 in., leaving a sensing length of 0·049 in. The gold-plated probe was found to produce more consistent results than an ordinary hot wire (DISA Type 55 F 31). This is perhaps due to the lower level of aerodynamic interference of the gold-plated probes.

Hollingsworth (1967) quotes the sensitivity of his method as $\pm 0{\cdot}1°$. It is difficult to estimate the accuracy of the technique. Some idea may be obtained from the scatter in the experimental data. A further check on the accuracy of the method is possible from the mass balance of the secondary flow. The net mass flow across any line drawn between the pipe wall and the pin surface or between the pipe wall and the axis of the symmetry must be zero. For a total of 15 radial traverses, the results show that the mass imbalance occurred with nearly equal frequency on the positive and negative side. The standard deviation of the error in mass balance, expressed as a percentage of the maximum value of the secondary-flow stream function, was found to be 9 %. In view of the small secondary flows present, this level of error is considered acceptable.

4. Results and discussion

4.1. *Friction factor*

For uniform-density fully developed channel flows, measurements of the pressure drop and mass-flow rate enable the friction factor f to be calculated according to the following formula:

$$f = \frac{(-dp/dx)\, d_e}{2\rho U_b^2}, \tag{2}$$

where d_e is the equivalent diameter of the duct, U_b is the bulk velocity for the duct, p is the static pressure measured at the pipe wall and x is the distance along the axis of the duct.

In fully developed channel flows, dp/dx is constant, and the most common cause of error in the determination of the friction factor is inaccuracy in the measurement of the mass-flow rate. In concentric-annulus experiments, Lawn & Elliott (1972) have checked the calibration of the flow meter used in the present work. As an additional check, experimentally measured velocity profiles were integrated for Reynolds numbers of $2{\cdot}15 \times 10^5$ and $6{\cdot}37 \times 10^4$ to obtain the mass-flow rates. The values calculated in this way agreed to within 1 % with the mass-flow rates obtained from the orifice meter. In view of this good agreement it is

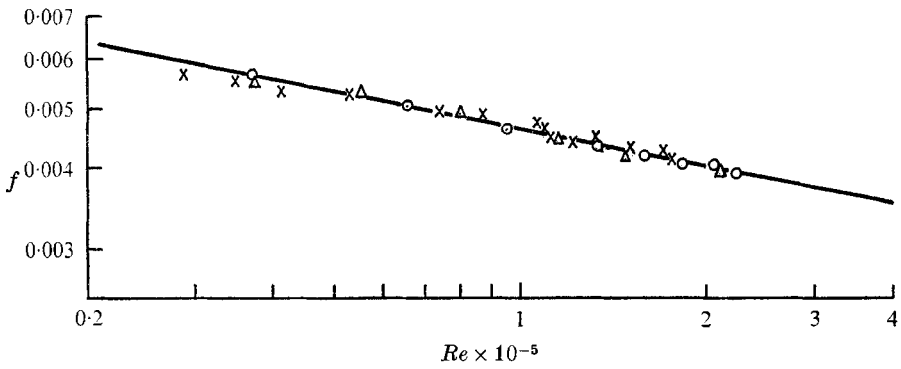

FIGURE 4. Friction-factor results. Present data: ○, single pin (eccentric); ×, two pins. △, single pin (concentric; Lawn & Elliott 1972). ——, best-fit line for present data, $f = 0{\cdot}0445Re^{-0{\cdot}196}$.

estimated that the present results for the friction factor are correct to within 2% at the highest Reynolds numbers. At lower Reynolds numbers the error could be between 3 and 4%, owing to slightly more scatter in the pressure measurements and some inaccuracies in the orifice-meter calibration at very low mass-flow rates.

Friction-factor results for the single-pin and two-pin experiments are presented in figure 4. Friction-factor data for the two-pin case are within 2% of the single-pin data. This difference is of the same order as the experimental error, and it can be concluded that, if the equivalent diameter is used as the reference length, the relationship between the friction factor and Reynolds number for both flows may be taken as

$$f = 0{\cdot}0445\,Re^{-0{\cdot}196}, \tag{3}$$

where $Re = U_b d_e/\nu$. This equation gives friction factors which are approximately 5% higher than Lawn's (1970) data for pipe flow.

From the results of Jonsson & Sparrow (1966) it is possible to interpolate the friction factors to predict values for the present eccentricity. Their interpolated results agree to within 2% with the present single-pin data. Figure 4 also shows the data of Lawn & Elliott (1972) for a concentric-annulus experiment. Because of the small eccentricity in the present experiment, close agreement between Lawn & Elliott's data and the present data for a single pin is to be expected.

4.2. *Shear stress distribution*

The shear stress distribution on the pipe wall was obtained from Clauser's (1956) chart with the assumption of a 'universal' velocity profile, which may be written as

$$U^+ = A \ln y^+ + B. \tag{4}$$

The constants A and B were chosen in accordance with the recommendation of Patel (1965). It is estimated that the accuracy of the Clauser chart in the determination of the shear stress is about 4% and 2% at Reynolds numbers of $3{\cdot}7 \times 10^4$ and $2{\cdot}15 \times 10^5$ respectively. The loss in accuracy at the lower Reynolds

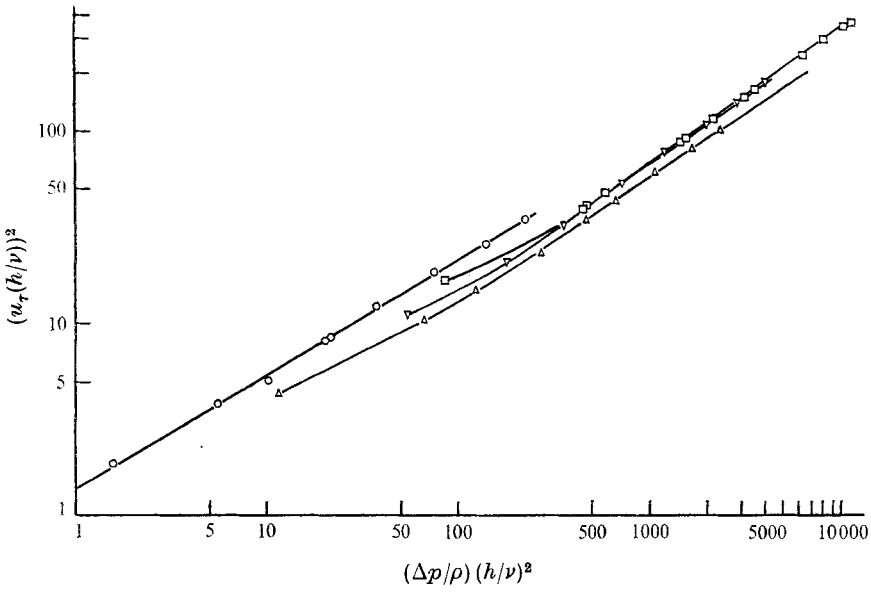

FIGURE 5. Calibration curves for skin-friction fences.

	○	△	▽	□
Fence code name	*A* 2	*A* 3	*A* 4	*A* 1
h (in.)	0·0026	0·0043	0·0057	0·0083

number is due to slightly higher random error in the velocity measurements. Because the velocity profiles are not universal near the pin surface, they cannot be used to determine the local shear stress on the pin. As was mentioned earlier, a calibrated boundary-layer fence was used to determine the shear stress distribution.

From dimensional arguments, the pressure difference across a fence submerged in a boundary layer may be correlated according to the following expression:

$$\frac{\Delta p}{\rho}\left(\frac{h}{\nu}\right)^2 = f\left[\left(u_\tau \frac{h}{\nu}\right)^2\right], \tag{5}$$

where Δp is the pressure drop across the boundary-layer fence and h is the height of the fence.

The form of the function is usually determined by experiment. Bradshaw & Gregory (1959), Hool (1956), Gadd (1960) and Trilling & Hakkinen (1955) found that $\Delta p \propto \tau_s^b$.

In order to obtain the calibration curves, the concentric annulus set up by Lawn & Elliott (1972) was used. Lawn & Elliott determined the shear stress on the pin by experimentally locating the zero-shear plane and performing a force balance on the flow area between the pin and the zero shear stress. They estimated a maximum error of 2 % in the pin shear stress. In the present work the calibration curve for a given fence was obtained by recording the pressure drop Δp across the fence at various mass-flow rates. The values of Δp were related to the pin shear stress using the results of Lawn & Elliott (1972).

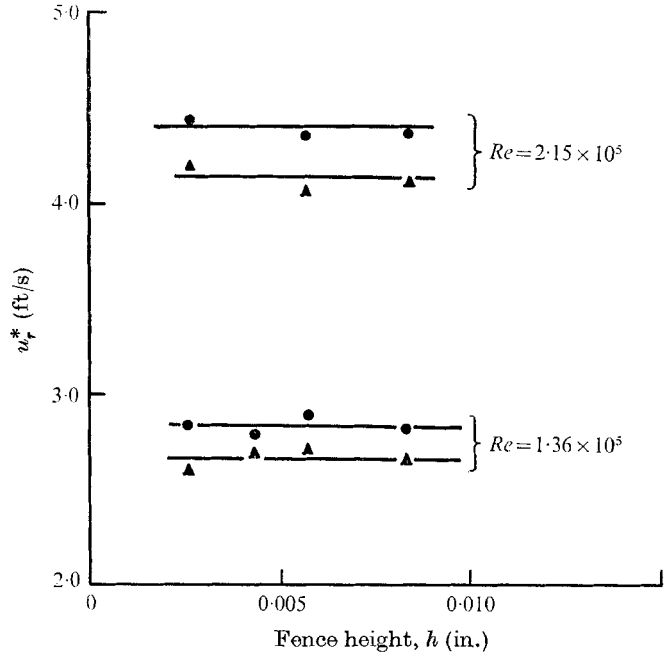

FIGURE 6. Friction velocities as measured by fences of different height in the single-pin experiment. ▲, $\theta^* = 0$; ●, $\theta^* = 180°$.

Figure 5 shows the calibration curves for four boundary-layer fences. For the smallest fence height of 0·0026 in., b is approximately 1·7 and for the other fences an average value of 1·5 may be taken. This is in good agreement with the data of Bradshaw & Gregory (1959). The slight shift in calibration curves for different fences is due to some inaccuracy in the determination of h. This will not affect the accuracy of the shear stress measurements as all the fences were individually calibrated.

Single-pin data. The shear stress distribution on the pin surface was obtained using all four different fences. Figure 6 shows the results at Reynolds numbers of $2{\cdot}15 \times 10^5$ and $1{\cdot}36 \times 10^5$ for $\theta^* = 0$ and 180° (where θ^* is the azimuthal angle measured at the centre of the rod, see figure 1). The maximum deviation in the local friction velocity u_r^* on the rod surface is not more than 2·5 % for a nearly fourfold variation in the fence height. After this check that all the fences gave consistent results, subsequent runs were done with fence A 1, which had $h = 0{\cdot}0083$ in.

Normalized shear stress distributions on the pin surface and the pipe wall at Reynolds numbers of $2{\cdot}15 \times 10^5$, $1{\cdot}36 \times 10^5$, $6{\cdot}37 \times 10^4$ and $3{\cdot}7 \times 10^4$ are shown in figure 7. The average shear stresses $\overline{u_r^*}$ and $\overline{u_p^*}$ for the rod and pipe surface, respectively, were derived from integrating the shear stress distributions obtained using the fence. It is interesting to note that the maximum shear stress on the pin does not occur at $\theta^* = 180°$ but at $\theta^* = 120°$. Similar behaviour was noted by Leutheusser (1963) in square ducts. He found that the point of maximum shear stress occurs nearly half way between the corner of the duct and the centre

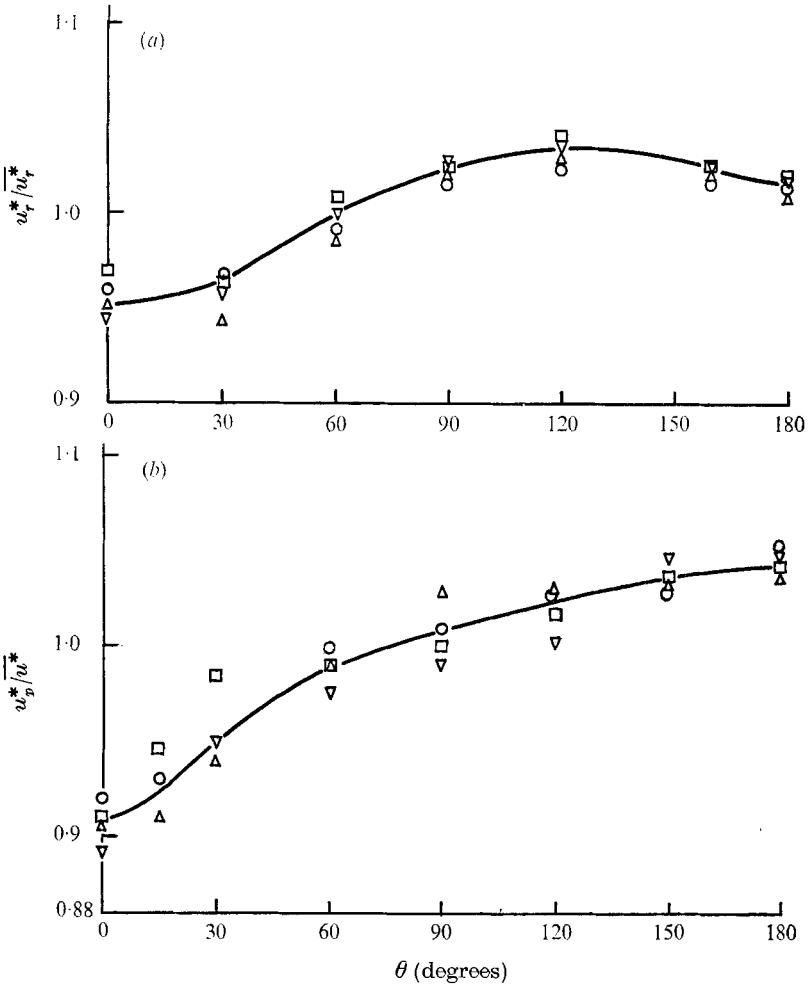

FIGURE 7. Shear stress distributions on (*a*) the pin surface and (*b*) the pipe wall for the single-pin experiment. ——, mean line through experimental points.

	○	△	▽	□
$Re \times 10^{-5}$	2·15	1·36	0·637	0·373
(*a*) $\overline{u_\tau^*}$ (ft/s)	4·29	2·78	1·47	0·96
(*b*) $\overline{u_p^*}$ (ft/s)	3·794	2·52	1·31	0·786

of the duct side. The normalized shear stress distributions on the pipe wall and pin surface do not show any systematic trend with respect to Reynolds number. On the pipe wall, the maximum shear stress occurs at $\theta = 180°$, and is nearly 13 % higher than the shear stress at $\theta = 0$.

Two-pin data. Since no Reynolds-number dependence was observed for the single-pin experiment, the shear stress distributions for the two-pin duct were obtained at the Reynolds number of $1{\cdot}77 \times 10^5$ only. The shear stress distributions around the two pins agreed to within 2 %. This shows that the flow was symmetrical in the four quadrants. Figure 8 shows the normalized shear stress distribution around the pin for positive and negative values of θ^*; the two

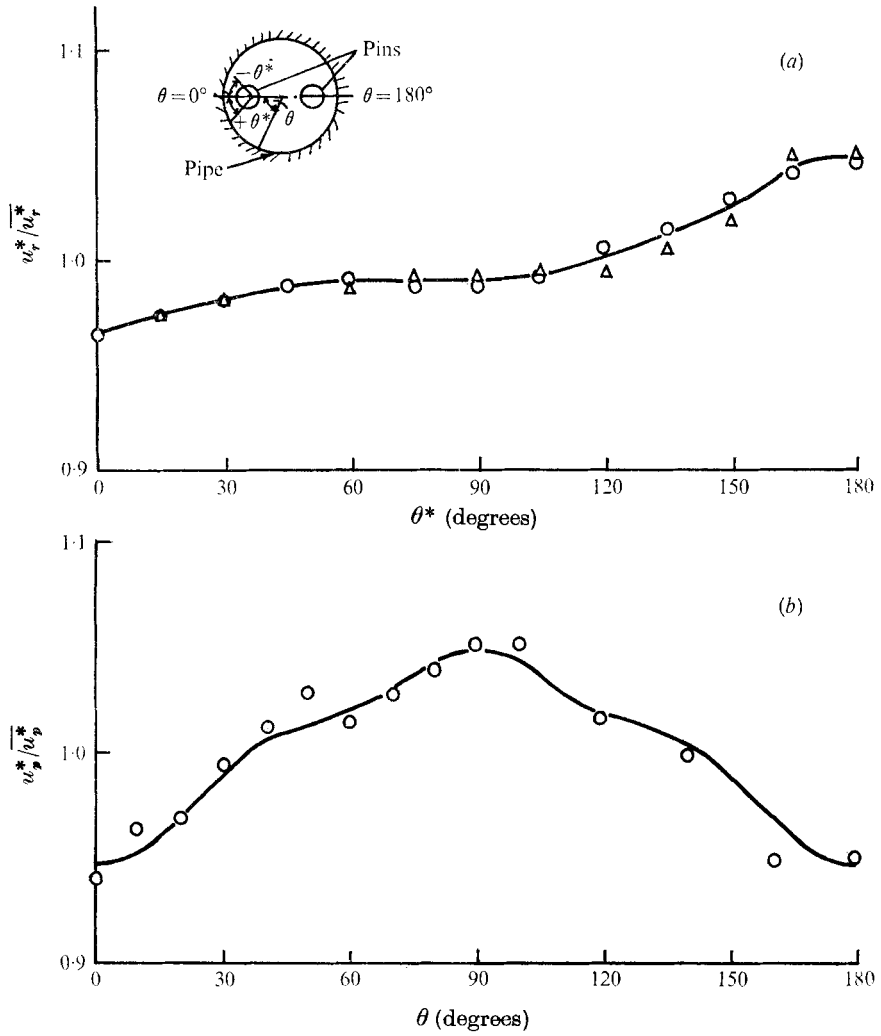

FIGURE 8. Shear stress distributions on (*a*) the pin surface and (*b*) the pipe wall for the two-pin experiment; $Re = 1{\cdot}77 \times 10^5$. (*a*) ○, $-\theta^*$; △, θ^*; ——, mean line through experimental points; $\overline{u_r^*} = 4{\cdot}364$ ft/s. (*b*) ○, experimental points; ——, mean line through experimental points; $\overline{u_p^*} = 3{\cdot}8$ ft/s.

distributions agreed well with each other. Figure 8 also shows the normalized shear stress on the pipe surface.

It is interesting to compare the shear stress distributions for the single-pin and two-pin ducts. For the two-pin geometry, the maximum shear stress on the pin occurred at $\theta^* = 180°$ as compared with $\theta^* = 120°$ in the case of the single-pin and the shear stress distribution between $\theta^* = 45°$ and 120° was more uniform. The maximum variation in the pipe-surface shear stress was only 10 % in this case, as compared with 13 % for the single-pin case.

Accuracy. The shear stress distributions presented in figures 7 and 8 can be used to calculate the average frictional forces acting on the pipe wall and the

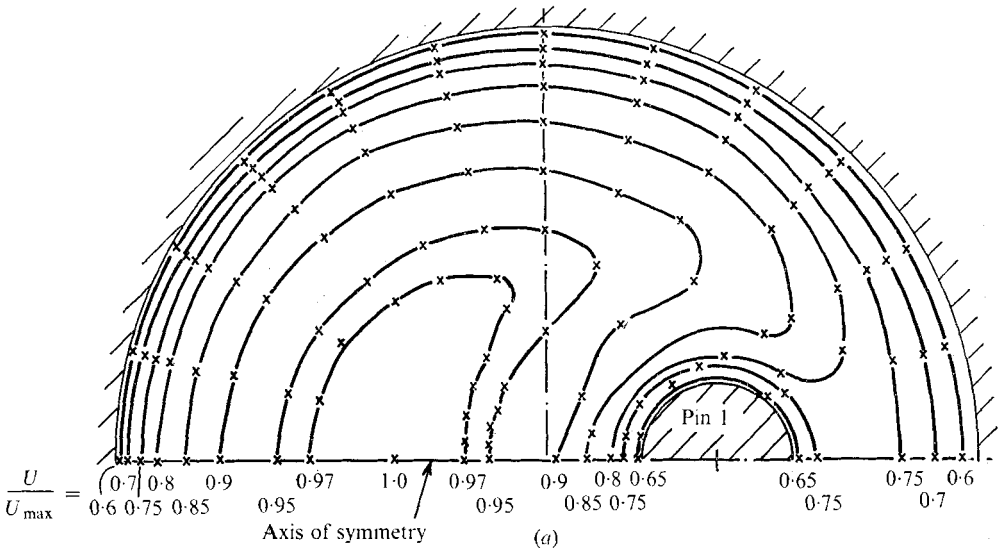

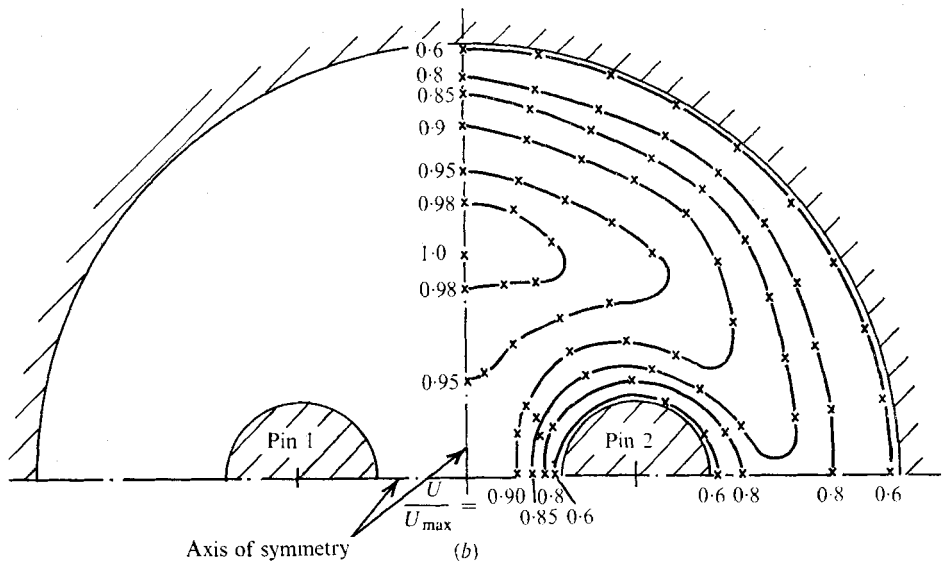

FIGURE 9. Axial-velocity contours. (*a*) $Re = 2{\cdot}15 \times 10^5$, $U_{max} = 104{\cdot}5$ ft/s, $U_{max}/U_b = 1{\cdot}17$. (*b*) $Re = 1{\cdot}77 \times 10^5$, $U_{max} = 94{\cdot}5$ ft/s, $U_{max}/U_b = 1{\cdot}15$.

pin surface. For fully developed uniform-density duct flows, the sum of frictional forces must be balanced by the pressure gradient. In the present investigation, the maximum error in the force balance was 3 %.

4.3. *Velocity distributions*

Velocity profiles for the single-pin experiment were obtained at four Reynolds numbers: $2{\cdot}15 \times 10^5$, $1{\cdot}35 \times 10^5$, $0{\cdot}637 \times 10^5$ and $0{\cdot}379 \times 10^5$. It is convenient to present the velocity profiles as plots of equivelocity contours, usually called 'isovels'. The general shape of the contour plots is very similar for different Reynolds numbers. However, the ratio of the maximum velocity to the bulk velocity ($U_{\max}/U_b$) was 1·13 at $Re = 2{\cdot}15 \times 10^5$, as compared with 1·16 at $Re = 0{\cdot}37 \times 10^5$. This suggests that a higher Reynolds number the flow is more uniform. A similar trend was observed by Ying (1971) in square ducts, Lawn & Elliott (1972) in concentric annuli and Lawn (1970) in a circular pipe.

For the case of the two-pin geometry, the isovel contour plot was obtained at a Reynolds number of $1{\cdot}77 \times 10^5$ only. Since the flow was symmetrical in the four quadrants, velocity profiles were obtained in only one quadrant. However, the symmetry of the velocity profiles was checked and found to be not worse than ± 1 % in either experiment, being slightly better than this in the single-pin case.

Velocity contour plots are presented in figure 9 for the single-pin and two-pin cases at Reynolds numbers of $2{\cdot}15 \times 10^5$ and $1{\cdot}77 \times 10^5$ respectively. The locations and magnitudes of the maximum velocities are shown in the diagram.

Velocity profiles normal to the pin surface are presented in non-dimensional U^+, y^+ co-ordinates in figure 10(*a*) for the single-pin geometry at $Re = 2{\cdot}15 \times 10^5$ and in figure 10(*b*) for the two-pin case at $Re = 1{\cdot}77 \times 10^5$. A line representing the universal law of the wall $U^+ = 5{\cdot}5 \log_{10} y^+ + 5{\cdot}45$ is shown in each figure. The deviations from the universal law of the wall are smallest for $\theta^* = 30°$ and 60°. In general, the velocity profiles deviate more from the universal law of the wall in the two-pin geometry than in the single-pin case. These deviations can be attributed to the following.

(i) The effect of the radius of curvature, characterized by y/Rr. This embraces the effect of rapidly falling shear stress near the surface, as well as any 'direct' effect of curvature on the velocity profile.

(ii) Secondary flows. The Reynolds number $u_r^* R_r/\nu$ did not differ by more than 5 % in the two cases so the law of the wall would be expected to hold in the same range of y^+. It may be concluded that the secondary flow has some influence on the U^+, y^+ curve, because the differences in U^+ between the two cases and between different azimuthal positions in the range $y^+ \leqslant 100$ ($y/R_r \lesssim 0{\cdot}1$) are significant.

For the single-pin geometry, further U^+, y^+ curves were obtained at Reynolds numbers of $1{\cdot}35 \times 10^5$ and $0{\cdot}637 \times 10^5$; these were found to be similar to the velocity profiles at $Re = 2{\cdot}15 \times 10^5$. Within the range of the experiments, $u_r^* R_r/\nu$ was varied from 350 to 1100 and no systematic trend could be noted in the U^+, y^+ curve. In order to 'decouple' the shear stress variation from any possible effects which are directly related to the surface curvature, it would be necessary to test a range of radius ratios (see Lawn & Elliott 1972).

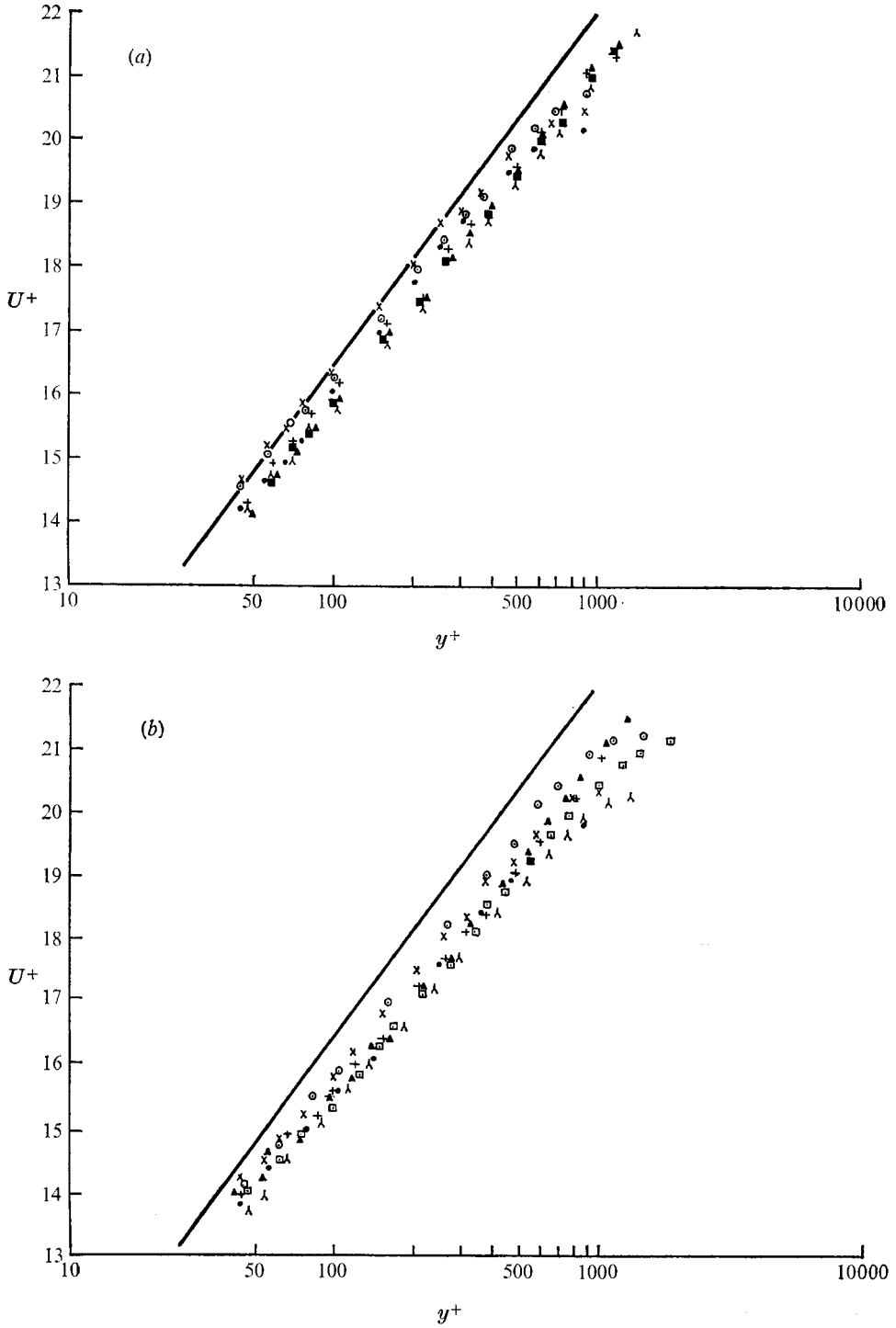

FIGURE 10. Pin surface velocity profiles in (*a*) single-pin and (*b*) two-pin experiment. ——, $U^+ = 5{\cdot}5 \log_{10} y^+ + 5{\cdot}45$. (*a*) $Re = 2{\cdot}15 \times 10^5$. (*b*) $Re = 1{\cdot}77 \times 10^5$.

θ^* (degrees)	● 0	× 30	⊙ 60	+ 90	▲ 120	⊡ 150	λ 180

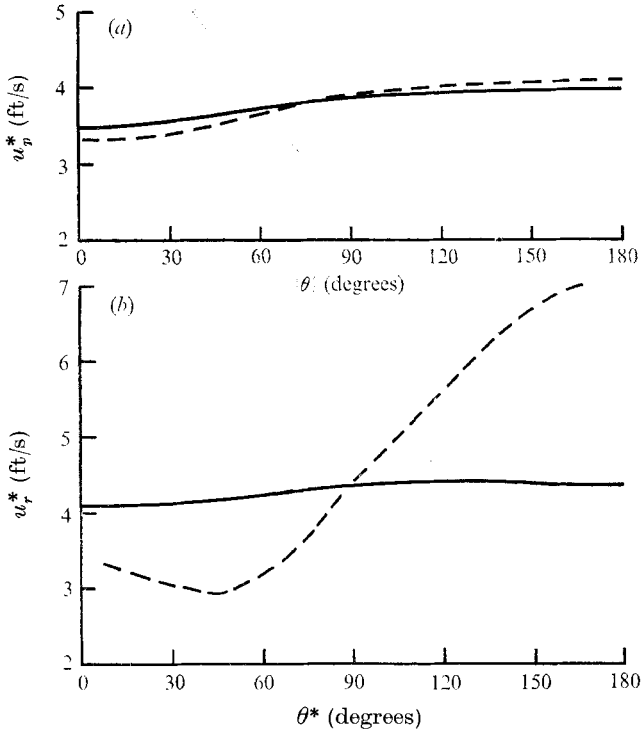

FIGURE 11. Comparison between present shear stress results and the shear stress calculated using Jonsson & Sparrow's method for single-pin geometry. ——, mean line through present experimental results; – –, Jonsson & Sparrow's method. (*a*) Pipe surface. (*b*) Pin surface.

4.4. *Jonsson & Sparrow's method for the calculation of shear stress distribution*

Jonsson & Sparrow (1966) employed velocity contour diagrams for the calculation of the shear stress distribution on the pipe wall and pin surface. They assumed that the shear stress is zero on the lines normal to isovels and on the maximum-velocity surface. By a force balance with the pressure gradient acting on flow areas enclosed by the walls and zero-shear surfaces, they then obtained the shear stress distribution on the pipe wall and pin surface. They also had to assume that there are no secondary flows: i.e. no transfer of mean-flow momentum takes place across the lines deemed to be those of zero shear. Figure 11 shows the comparison between the experimentally measured shear stress distribution and the shear stress distribution calculated using Jonsson & Sparrow's method. On the pipe wall the agreement between the experiments and the calculations is reasonable. However, on the pin surface the calculations predict a much larger variation in the shear stress than that observed experimentally. This discrepancy was significant enough to warrant a closer look at the assumptions made by Jonsson & Sparrow. The three factors which may be responsible for the discrepancy between the experiments and the calculations are as follows.

(i) The surface on which the velocity is a maximum is not necessarily that on

which the shear stress is zero. Lawn & Elliott's data (1972) for concentric annuli and Kacker's data (1971) for the eccentric annulus are sufficient proof in this respect.

(ii) The planes normal to isovels have shear stresses acting on them. They cannot be neglected in a force balance.

(iii) It will be shown in the next section that secondary flows are present in the eccentric annulus which transfer mean momentum across the planes of zero shear, the planes of maximum velocity and the planes which are normal to the isovels. The secondary flows are generated in such a way as to make the shear stress distribution on the pin more uniform than the one obtained by the calculations of Jonsson & Sparrow.

4.5. *Secondary-flow distribution*

As was mentioned in § 3.3, the secondary-flow angles were measured using a method due to Hoagland (1960). All the traverses were normal to the pipe wall. The measured secondary-flow angle γ is related to the mean velocity U and the secondary-flow velocity W as follows:

$$W = U\tan(\gamma). \tag{6}$$

Secondary-flow velocities obtained from (6) were used to calculate a secondary-flow stream function ψ defined as follows:

$$W = \frac{\partial\psi}{\partial r}, \quad V = -\frac{1}{r}\frac{\partial\psi}{\partial\theta}, \tag{7}$$

where r denotes the radial distance of a point from the centre of the pipe.

Since V and W are continuous everywhere in the flow, ψ may be written in differential form as

$$d\psi = \frac{\partial\psi}{\partial r}dr + \frac{\partial\psi}{\partial\theta}d\theta. \tag{8}$$

In terms of V and W

$$d\psi = W\,dr - rV\,d\theta. \tag{9}$$

On integration (9) yields

$$\psi = \left|\int_0^r W\,dr\right|_{\theta=\text{constant}}, \tag{10}$$

or

$$= -\left|\int_0^\theta rV\,d\theta\right|_{r=\text{constant}}. \tag{11}$$

Only the distribution of W was measured, and from this the ψ distribution was calculated using (10). The present traversing system did not allow the velocity V to be measured: these measurements would of course have provided an additional check on the ψ distribution calculated from (11).

The secondary-flow angles were measured for the single-pin geometry at Reynolds numbers of $6{\cdot}37\times10^4$ and $2{\cdot}15\times10^5$. The flow angles in most of the flow field are typically of the order of $\frac{1}{2}°$. Near the pin, maximum flow angles of approximately 1° were measured. The distribution of secondary-flow velocities W is shown in figure 12. These have been normalized by the maximum friction

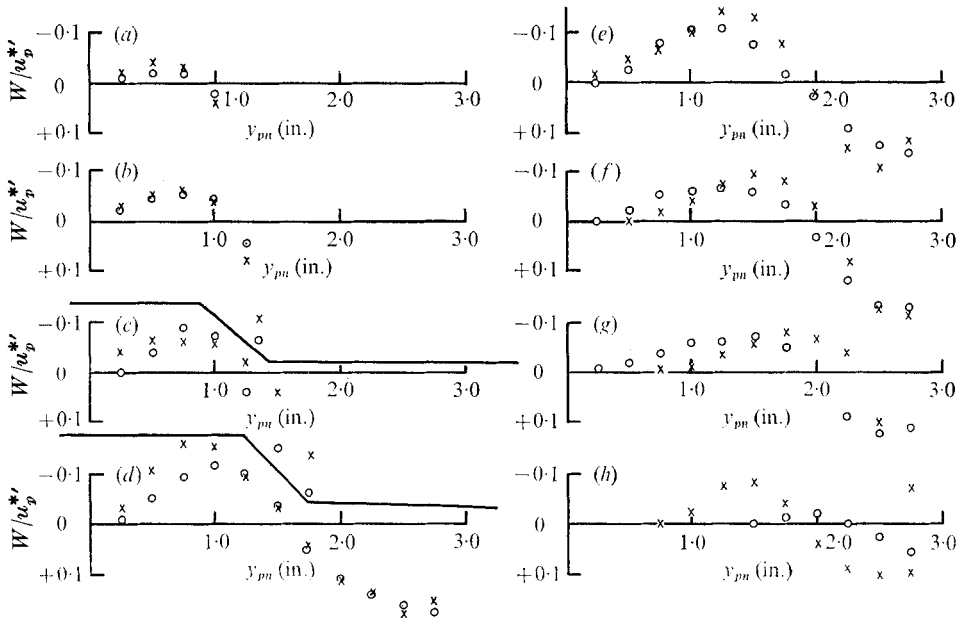

FIGURE 12. Secondary-flow velocities in the single-pin duct. ○, $Re = 6{\cdot}37 \times 10^4$; ×, $Re = 2{\cdot}15 \times 10^5$. (*a*) $\theta = 10°$. (*b*) $\theta = 20°$. (*c*) $\theta = 30°$. (*d*) $\theta = 45°$. (*e*) $\theta = 60°$. (*f*) $\theta = 90°$. (*g*) $= 120°$. (*h*) $\theta = 150°$.

velocity $u_p^{*\prime}$ measured on the pipe surface, which occurred at $\theta = 180°$. Within the experimental scatter there does not appear to be any trend in the distributions of $W/u_p^{*\prime}$ with Reynolds number. Since the ratio of $u_p^{*\prime}$ to $\overline{u^*}$ (where $\overline{u^*}$ is average friction velocity for the duct) is also independent of Reynolds number, it may be concluded that, if W profiles were to be normalized by the average friction velocity, the normalized curves would also be independent of Reynolds number.

Hoagland (1960) normalized his secondary velocities by the bulk velocity and found no dependence of Reynolds number. However, Gessner & Jones (1965) concluded that the friction velocity is a more appropriate scaling parameter. In the present investigation within the range of Reynolds number, $\overline{u^*}/U_b$ changes by only 12%.

The accuracy of W is not good enough to determine whether $\overline{u^*}$ or U_b is the proper scaling factor for the secondary velocities. Ying (1971) measured secondary velocities in a rough channel and a smooth one, and thus he was able to obtain a large variation of $\overline{u^*}/U_b$ (although the variation in Reynolds number was only four fold). His results show that the friction velocity is a better scaling parameter because the secondary-flow data of both the channels when normalized with the friction velocity give the same results.

The distribution of the secondary-flow stream function ψ is shown in figure 13 for Reynolds numbers of $6{\cdot}37 \times 10^4$ and $2{\cdot}15 \times 10^5$. The ψ distributions at the two Reynolds numbers are similar in shape; both have one circulating flow cell. The secondary flows are generated by turbulence in such a way as to take fluid

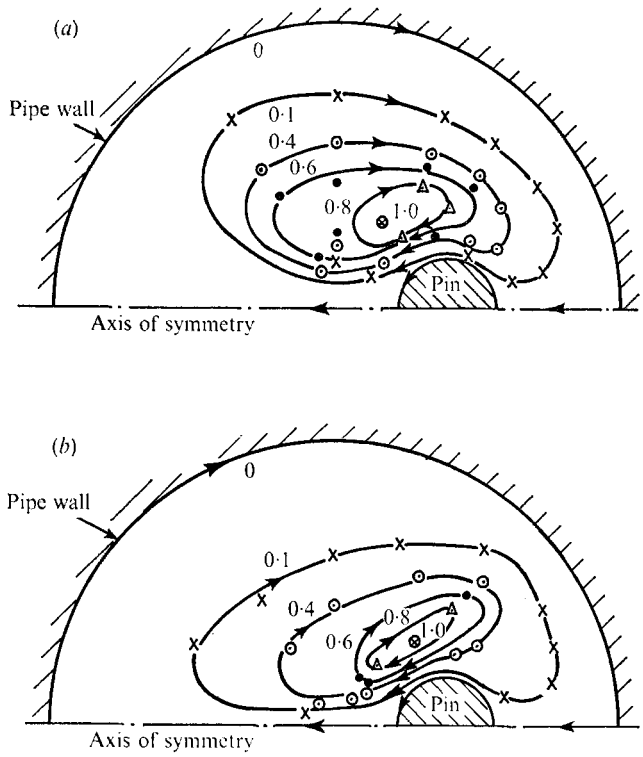

FIGURE 13. Secondary-flow streamlines at (*a*) $Re = 6{\cdot}37 \times 10^4$ ($\psi_{max} = 1{\cdot}23 \times 10^{-2}$ ft^2/s) and (*b*) $Re = 2{\cdot}15 \times 10^5$ ($\psi_{max} = 4{\cdot}8 \times 10^{-2}$ ft^2/s) for the single-pin geometry. ——, mean line through experimental points.

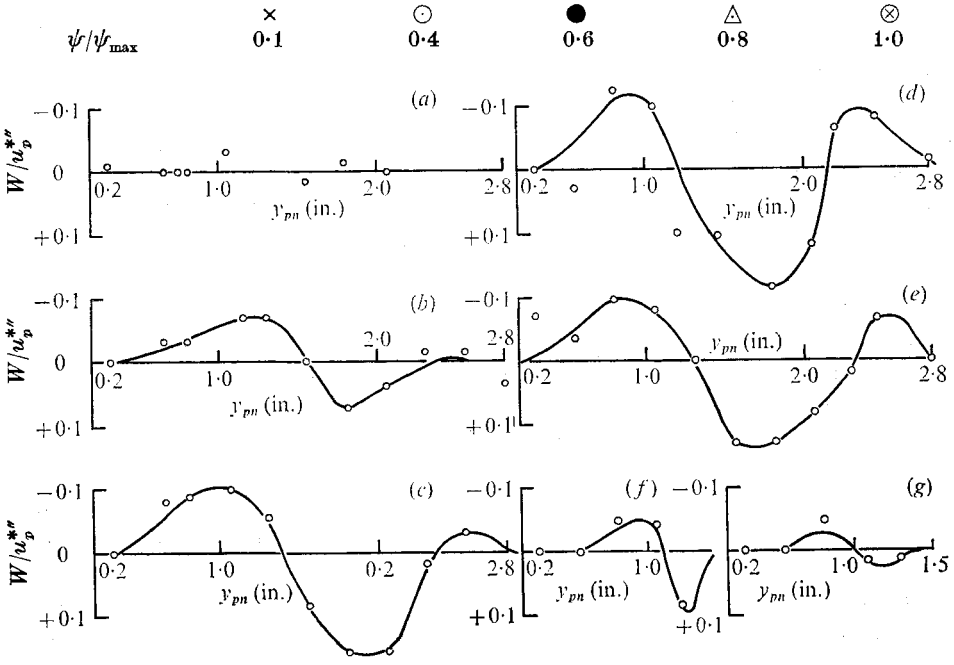

FIGURE 14. Measured secondary-flow velocities for the two-pin experiment at $Re = 1{\cdot}77 \times 10^5$ o, experimental points; ——, mean line through experimental points. (*a*) $\theta = 90°$. (*b*) $\theta = 80°$. (*c*) $\theta = 60°$. (*d*) $\theta = 50°$, (*e*) $\theta = 30°$. (*f*) $\theta = 20°$. (*g*) $\theta = 10°$.

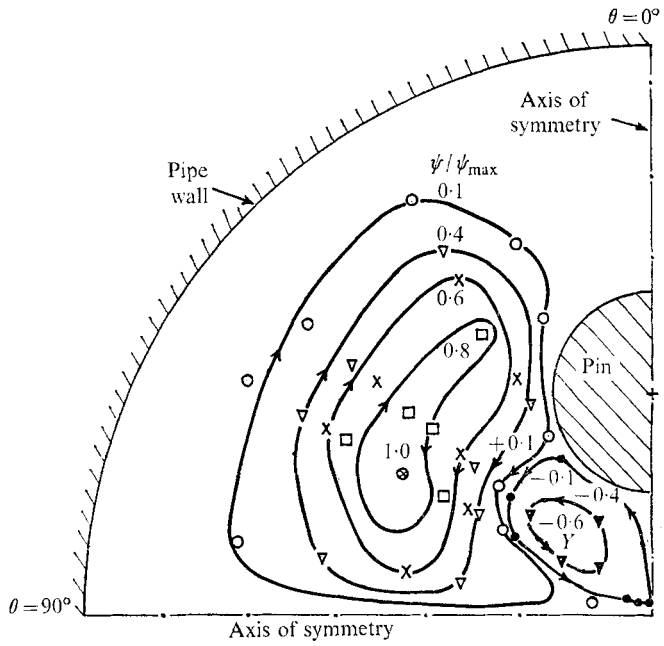

FIGURE 15. Distribution of secondary-flow stream function measured in the two-pin duct. (Only one quadrant shown.) ——, mean line through experimental points; $\psi_{max} = 0{\cdot}025\,\mathrm{ft^2/s}$; $Re = 1{\cdot}77 \times 10^5$.

	Y	▼	●	○	▽	×	□	⊗
ψ/ψ_{max}	−0·6	−0·4	−0·1	0·1	0·4	0·6	0·8	1·0

momentum from the region of high velocity (largest gap at $\theta = 180°$) to the region of low velocity (smallest gap at $\theta = 0$). This pattern is similar to the stream function distribution observed in square ducts, where the secondary flow transfers the momentum from the centre of the duct to the corner region.

In the case of the two-pin geometry, secondary-flow angles were measured at a Reynolds number of $1{\cdot}77 \times 10^5$. The magnitude of the secondary-flow angles is of the same order as those obtained for the single-pin geometry. The normalized secondary-flow velocities are shown in figure 14. In this case the normalizing velocity is $u_p^{*\prime\prime}$, which is the maximum pipe wall friction velocity, at $\theta = 90°$. The distribution of the secondary-flow velocities and the flow angles in the two-pin case is different from the distribution obtained in the single-pin geometry. This is more obvious from the stream function distribution shown in figure 15. The figure shows that, in addition to the flow cell which is present in the single-pin geometry, one finds a second cell sandwiched between the centre of the pipe and the pin. The total flow in the second cell is nearly 60 % of the flow in the larger cell.

All the previous measurements of secondary flows (Hoagland 1960; Leutheusser 1963; Brundrett & Baines 1964; Ying 1971) were made in ducts having corners. Hoagland and Ying have reported hot-wire probe interference in the measurement of secondary flows in the presence of corners. Fortunately, present measurements of secondary flows do not suffer from any probe interference, and consequently they have a slightly better accuracy.

5. Conclusions

(i) The use of an equivalent diameter in the definition of the Reynolds number and friction factor enables the equation $f = 0{\cdot}0445\,Re^{-0{\cdot}196}$ to represent the data to within 2 % for both the single-pin and two-pin geometries. The friction-factor data for the single-pin case (or eccentric annulus) is nearly 5 % higher than the pipe friction factor (Lawn 1970).

(ii) The shear stress distribution on the pin and pipe surface, if normalized by the average surface shear stress, is independent of Reynolds number within the Reynolds-number range $3{\cdot}73 \times 10^4$ to $2{\cdot}15 \times 10^5$. For the single-pin and two-pin ducts, the shear stress variation on the pipe and the pin surface was typically of the order of 12 % and 8 % respectively. The very nearly uniform value of the wall shear stress around the core tube for the single-pin and two-pin arrangements is due to increased momentum transfer by the secondary flow.

(iii) Calculated shear stress distributions based upon Jonsson & Sparrow's (1966) method do not agree with the experimental shear stress distributions mainly because their method neglects momentum transfer by the secondary flows.

(iv) U^+, y^+ plots near the pin surface deviate from the universal law of the wall, typically by 6 % and 3 % for the two-pin and single-pin ducts respectively.

(v) Two secondary-flow cells were observed in the two-pin duct as compared to one in the single-pin case.

The work described in this paper was carried out at Berkeley Nuclear Laboratories, Central Electricity Generating Board, Berkeley, England. The author wishes to thank Mr C. J. Lawn of Berkeley Nuclear Laboratories for many useful discussions.

REFERENCES

Bradshaw, P. & Gregory, N. 1959 *Aero. Res. Counc R. & M.* no. 3203.

Brundrett, E. & Baines, W. D. 1964 *J. Fluid Mech.* **10**, 375.

Clauser, F. H. 1956 The turbulent boundary layer. In *Advances in Applied Mechanics*, vol. IV. Academic.

Gadd, G. E. 1960 *Aero. Res. Counc. R. & M.* no. 3147.

Gessner, F. B. & Jones, J. B. 1965 *J. Fluid Mech.* **23**, 689.

Hoagland, L. C. 1960 Sc.D. thesis, M.I.T.

Hollingsworth, P. D. 1967 *C.E.G.B. Rep.* RD/B/N892.

Hool, J. N. 1956 *Aircraft Engng*, **28**, 52.

Jonsson, V. K. & Sparrow, E. M. 1966 *J. Fluid Mech.* **25**, 65.

Kacker, S. C. 1971 *C.E.G.B. Rep.* RD/B/N2117.

Lawn, C. J. 1970 *C.E.G.B. Rep.* RD/B/R1575(A).

Lawn, C. J. & Elliott, C. J. 1972 *J. Mech. Engng Sci.* **14**, 195.

Leutheusser, H. J. 1963 *J. Hydraulic Div. Proc.* A.S.C.E. **89**, 3508.

MacMillan, F. A. 1956 *Ministry of Supply, Aero. Res. Counc. Rep.* no. 3028.

Patel, V. C. 1965 *J. Fluid Mech.* **23**, 185.

RAO, G. N. V. 1967 *J. Appl. Mech., Trans. A.S.M.E.* **34**, 237.

SKINNER, V. R., FREEMAN, A. R. & LYALL, H. G. 1969 *Int. J. Heat Mass Transfer*, **12**, 265.

STARR, J. B. & SPARROW, E. M. 1967 *J. Fluid Mech.* **29**, 495.

TRILLING, L. & HAKKINEN, R. J. 1955 *Jare Grenzschichtforschung*, p. 201. Braunschweig, Friedr, Vieweg.

YING, W. M. 1971 Ph.D. thesis, Imperial College, London.